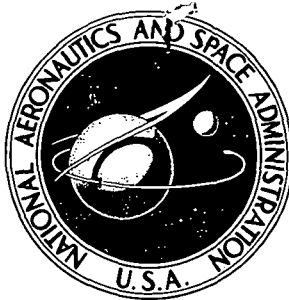


74N11812

**NASA TECHNICAL NOTE**



**NASA TN D-7446**

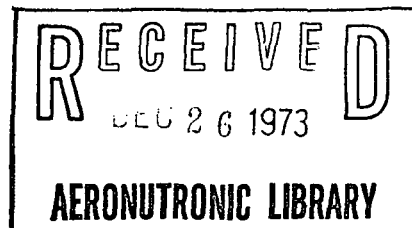
**NASA TN D-7446**

**EFFECT OF SUBSONIC INLET LIP GEOMETRY  
ON PREDICTED SURFACE AND FLOW  
MACH NUMBER DISTRIBUTIONS**

*by James A. Albers and Brent A. Miller*

*Lewis Research Center*

*Cleveland, Ohio 44135*



1. Report No. <b>NASA TN D-7446</b>	2. Government Accession No.	3. Recipient's Catalog No.	
4. Title and Subtitle <b>EFFECT OF SUBSONIC INLET LIP GEOMETRY ON PREDICTED SURFACE AND FLOW MACH NUMBER DISTRIBUTIONS</b>		5. Report Date December 1973	6. Performing Organization Code
		8. Performing Organization Report No. <b>E-7522</b>	10. Work Unit No. <b>501-24</b>
7. Author(s) <b>James A. Albers and Brent A. Miller</b>		11. Contract or Grant No.	
9. Performing Organization Name and Address <b>Lewis Research Center National Aeronautics and Space Administration Cleveland, Ohio 44135</b>		13. Type of Report and Period Covered <b>Technical Note</b>	
		14. Sponsoring Agency Code	
12. Sponsoring Agency Name and Address <b>National Aeronautics and Space Administration Washington, D. C. 20546</b>		15. Supplementary Notes	
16. Abstract <p>The effect of subsonic inlet lip geometry on predicted surface and flow Mach number distributions is illustrated. The theoretical results were obtained from incompressible potential flow calculations corrected for compressibility. The major emphasis of this investigation is on the low-speed (takeoff and landing) operating conditions. The low-speed results were obtained for a range of three geometric variables of interest: contraction ratio, defined as the ratio of highlight area to throat area; internal lip major- to minor-axis ratio; and internal lip shape. The low-speed results were obtained at both static conditions and a free-stream velocity of 42.6 m/sec, with incidence angles ranging from 0° to 50°. The results indicate that of the three geometric variables considered, contraction ratio had the largest effect on the surface Mach number distributions. The effects of inlet diameter ratio and blunting of the external forebody on maximum external surface Mach numbers are illustrated at a cruise Mach number of 0.8.</p>			
17. Key Words (Suggested by Author(s)) <b>Engine inlets                      Nacelles Induction system                Pressure distribution Potential flow Inlet flow</b>		18. Distribution Statement <b>Unclassified - unlimited</b>	
19. Security Classif. (of this report) <b>Unclassified</b>	20. Security Classif. (of this page) <b>Unclassified</b>	21. No. of Pages <b>36</b>	22. Price* <b>Domestic, \$3.00 Foreign, \$5.50</b>

# EFFECT OF SUBSONIC INLET LIP GEOMETRY ON PREDICTED SURFACE AND FLOW MACH NUMBER DISTRIBUTIONS

by James A. Albers and Brent A. Miller

Lewis Research Center

## SUMMARY

The effect of subsonic inlet lip geometry on predicted surface and flow Mach number distributions is illustrated. The theoretical results were obtained from incompressible potential flow calculations corrected for compressibility. The major emphasis of this investigation is on the low-speed (takeoff and landing) operating conditions. The low-speed results were obtained for a range of three geometric variables of interest: contraction ratio, defined as the ratio of highlight area to throat area; internal lip major-to minor-axis ratio; and internal lip shape. The low-speed results were obtained at both static conditions and a free-stream velocity of 42.6 m/sec with incidence angles ranging from  $0^\circ$  to  $50^\circ$ . The results indicate that of the three geometric variables considered, contraction ratio had the largest effect on the surface Mach number distributions. The effects of inlet diameter ratio and blunting of the external forebody on maximum external surface Mach numbers are illustrated at a cruise Mach number of 0.8.

## INTRODUCTION

The propulsive and aerodynamic requirements imposed on short-haul (STOL) aircraft require the engine inlet to perform with good efficiency over a wide range of operating conditions. For short-haul aircraft, high engine thrust and aerodynamic lift are required at both takeoff and landing. Thus, the inlet must deliver airflow with a high total pressure recovery and low distortion while it is being subjected to large upwash and/or crossflow angles (ref. 1). This same inlet must then perform efficiently at cruise Mach numbers ranging from 0.6 to 0.8. One of the most important components of a subsonic inlet is the entry lip (ref. 2), since its geometry determines the flow conditions at the diffuser entrance. Little analytical or experimental information on flow distributions on nacelle inlets at high flow angles is available in the literature.

This report presents the results of an analytical study to investigate the effects of engine inlet lip geometry on internal and external surface Mach numbers and internal flow field Mach numbers. The Mach number profiles obtained can aid in the selection of an inlet lip design for a particular range of operating conditions. The general validity of the analytical technique was verified in reference 3, where the surface Mach numbers measured in a wind tunnel test (ref. 4) were shown to be in good agreement with the theoretically predicted values.

The major emphasis of this study is on the low-speed (takeoff and landing) operating conditions. The inlet lip geometric variables investigated are contraction ratio, major-to-minor-axis ratio, and the shape of the inlet lip surface (super-ellipse exponent used to generate lip surface). The effects of inlet diameter ratio and of blunting the external forebody on the maximum external surface Mach number at a cruise Mach number of 0.8 are illustrated. For all low-speed conditions investigated the one-dimensional throat Mach number was 0.71, which is representative of a takeoff power setting.

## ANALYSIS

The principal geometric variables for the inlet are illustrated in figure 1. For the inlets investigated the ratio of throat diameter to maximum diameter was constant, at  $D_T/D_{max} = 0.731$ . (All symbols are defined in appendix A.) The internal diameter downstream of the throat was constant. The ratio of external forebody length to maximum diameter was also constant, at  $L/D_{max} = 0.375$ . The length of the external forebody  $L$  was selected to give realistic values of the drag divergence Mach number for cruise performance for the inlet. The external diameter downstream of the forebody length was a constant value equal to  $D_{max}$ .

Theoretical Mach number distributions were calculated on the inlet surface from the stagnation point on the inlet lip to a reference plane in the inlet duct (fig. 1). The surface distance between the stagnation point and the reference plane  $s_{max}$  was used to nondimensionalize surface length. This surface length is nearly independent of inlet geometry if, as in the present analysis, the distance between the highlight and the reference plane  $W$  is constant.

The lip geometries were generated by super-ellipse curves of the form

$$\left(\frac{x}{a}\right)^n + \left(\frac{y}{b}\right)^n = 1 \quad (1)$$

where  $a$  and  $b$  are, respectively, the major and minor axis of the super-ellipse and  $n$  is the super-ellipse exponent. The lip geometry was represented by three geometric variables. They are the inlet contraction ratio, defined as the ratio of highlight area to

throat area  $A_1/A_T$ ; the major- to minor-axis ratio  $a/b$ ; and the super-ellipse exponent  $n$ . All the inlet lip geometric variables considered in this investigation are given in table I. This report considers inlet contraction ratios ranging from 1.30 to 1.42 (fig. 2(a)). The major- to minor-axis ratio  $a/b$  was varied from 1.5 to 3.0 (fig. 2(b)). For a given contraction ratio,  $a/b$  was varied by changing the value of  $a$  and holding  $b$  constant. This report considers values of the super-ellipse exponent  $n$  from 1.75 to 2.5 (fig. 2(c)).

The external forebody shape was also obtained by use of a super-ellipse curve. The super-ellipse exponent of the external forebody, denoted by  $m$ , was varied from 1.78 (approximate NACA-1 forebody contour) to 1.95 and 2.15 (blunter than a NACA-1 forebody contour). A comparison of the three external forebody shapes investigated is shown in figure 3. The external forebody shapes are plotted as fraction of thickness  $y/Y$  against fraction of length  $x/L$ . The table in figure 3 shows forebody minor- to major axis ratio  $Y/L$  as a function of inlet contraction ratio.

The theoretical Mach number distributions for the inlet geometries were obtained from incompressible potential flow calculations corrected for compressibility. The incompressible potential flow solution was obtained by using the method of reference 5. This method is based on the Douglas axisymmetric incompressible potential flow method (ref. 6). The compressibility correction of reference 7 was used to correct the incompressible results. Details of the method of solution are given in appendix B.

The theoretical Mach number distributions can be used to qualitatively compare the performance of various inlet geometries. The factors that influence inlet lip performance are (1) the maximum surface Mach number; (2) the average, or overall, adverse surface Mach number gradient; and (3) the local adverse Mach number gradient. The adverse Mach number gradients on the inlet lip are important when considering the growth and/or separation of the surface boundary layer. Some general design criteria are to minimize the peak Mach number and local and average Mach number gradients on the surface of the lip in order to minimize the thickness of the boundary layer and to avoid flow separation in the vicinity of the lip.

The Mach number distributions along the lip surface are presented in terms of a nondimensional surface length  $s/s_{\max}$  (fig. 1). The Mach number gradient for any scaled inlet size can be found from the scaling relation

$$\frac{dM}{ds} = \left[ \frac{dM}{d(s/s_{\max})} \right] \left( \frac{D_T}{s_{\max}} \right) \frac{1}{D_T} \quad (2)$$

where the scaled inlet throat diameter  $D_T$  is known and the quantities  $dM/d(s/s_{\max})$  and  $D_T/s_{\max}$  can be obtained from the figures presented.

## RESULTS AND DISCUSSION

The effect of inlet contraction ratio, lip major- to minor-axis ratio, and internal lip super-ellipse exponent on the internal surface and flow Mach number distributions are discussed first. This is followed by a discussion of the effect of external forebody shape on the internal and external Mach numbers.

### Effect of Inlet Contraction Ratio

Surface Mach number distributions are presented in figure 4 for static conditions and at a free-stream velocity of 42.6 m/sec with incidence angles of  $0^\circ$ ,  $30^\circ$ , and  $40^\circ$ . The Mach number distributions are presented from the stagnation point on the inlet ( $s = 0$ ) to the reference plane in the inlet duct  $s_{\max}$  (fig. 1). The inlet contraction ratio  $A_1/A_T$  was varied by changing the highlight diameter (fig. 2(a)). Thus, when the contraction ratio increases, the diameter ratio  $D_1/D_{\max}$  increases. All other geometric variables were kept constant. The internal lip major- to minor-axis ratio and super-ellipse exponent were both 2.0, and the external forebody was an approximate NACA-1 contour. All Mach number distributions for incidence angles  $\alpha$  other than zero are for the windward side of the inlet ( $\psi = 0^\circ$ ). This is the circumferential location of the maximum surface Mach number.

For static conditions (fig. 4(a)) and for incidence angles of  $30^\circ$  and  $40^\circ$  (figs. 4(c) and (d)), the maximum Mach number occurs very near the inlet highlight ( $x = 0$ ) location. For an incidence angle of  $0^\circ$  (fig. 4(b)) the maximum Mach number occurs downstream of the inlet highlight. For high-incidence-angle cases (figs. 4(c) and (d)) the Mach number immediately following the inlet highlight location (for  $A_1/A_T \geq 1.38$ ) decreases slightly and then increases. This unusual characteristic is attributed to the large changes of curvature around the inlet highlight. This result was obtained for the larger-contraction-ratio inlets even when very small coordinate point spacing was used around the inlet highlight.

Examination of figures 4(a), (c), and (d) indicates a reduction in the average adverse Mach number gradient on the inlet surface as the contraction ratio is increased from 1.3 to 1.42. For a given contraction ratio the average adverse Mach number gradient increases as incidence angle increases from  $0^\circ$ . The effect of contraction ratio is largest for the high incidence angle (fig. 4(d)).

Examination of figure 4 indicates the maximum local adverse surface Mach number gradient occurs very near the throat location for most conditions investigated. There is little difference in the surface Mach number gradient at the throat location as contraction ratio is increased from 1.3 to 1.42.

The values of maximum surface Mach number from figure 4 are crossplotted in

figure 5 as a function of contraction ratio. The maximum surface Mach number is highest for the lowest-contraction-ratio inlet. A maximum surface Mach number of 1.95 was obtained for the 1.3 contraction ratio lip at an incidence angle of  $40^\circ$ . The lowest value of maximum surface Mach number, 0.92, was obtained for the 1.42 contraction ratio lip at an incidence angle of  $0^\circ$ . At an incidence angle of  $40^\circ$ , there is a 27 percent reduction in maximum surface Mach number as contraction ratio is increased from 1.3 to 1.42.

The effect of inlet contraction ratio on the maximum surface Mach number for circumferential angles of  $0^\circ$  and  $180^\circ$  is illustrated in figure 6(a) for an incidence angle of  $30^\circ$ . The 1.3-contraction-ratio inlet shows the greatest circumferential variation in surface Mach number, from 1.64 at  $0^\circ$  to 0.8 at  $180^\circ$ . For a contraction ratio of 1.42 the Mach number varies from 1.22 at a  $\psi$  of  $0^\circ$  to 0.75 at a  $\psi$  of  $180^\circ$ . However, at the throat location the effect of contraction ratio on the circumferential variation of Mach number is substantially diminished (fig. 6(b)). The surface Mach number varies from 1.1 at a  $\psi$  of  $0^\circ$  to 0.72 at a  $\psi$  of  $180^\circ$  for a contraction ratio of 1.3. There is a 7 percent decrease in surface Mach number at a  $\psi$  of  $0^\circ$  as contraction ratio is increased from 1.3 to 1.42.

The effect of contraction ratio on the radial variation of Mach number at the throat plane is presented in figure 7. The Mach numbers are presented as a function of the non-dimensional radius ratio  $r/r_T$  from the inlet centerline. A  $r/r_T$  of 0 corresponds to the inlet centerline, and  $r/r_T$  of -1 and +1 correspond to the windward and leeward surfaces, respectively. For static conditions (fig. 7(a)) and a contraction ratio of 1.3, the Mach number varies from 0.575 on the inlet centerline to 0.925 on the inlet surface. For an incidence angle of  $30^\circ$  at a free-stream velocity of 42.6 m/sec, the passage Mach number distribution becomes skewed and a larger variation in Mach number exists across the throat plane (fig. 7(b)). For a contraction ratio of 1.3 the Mach number varies from 0.57 at a  $r/r_T$  of +0.36 to 1.1 at a  $r/r_T$  of -1.0. The highest-contraction-ratio inlet (1.42) has the lowest radial variation in Mach number for both the static and forward velocity conditions. The highest-contraction-ratio inlet has the longest distance from highlight to throat.

For low-speed considerations, it may be advantageous to vary the contraction ratio circumferentially so the Mach number gradient will be relatively constant around the circumference of the inlet at the design incidence angle.

#### Effect of Major- to Minor-Axis Ratio

The effect of major- to minor-axis ratio  $a/b$  on surface Mach number distribution is presented in figure 8 for static conditions and for 42.6-m/sec free-stream velocity and  $30^\circ$  incidence angle. Contraction ratio was varied over the range 1.3 to 1.42. The lip geometries corresponding to the different  $a/b$  ratios are illustrated in figure 2(b) for

a fixed contraction ratio. Examination of figure 8 indicates a large variation in surface Mach number profile as  $a/b$  ranges from 1.5 to 3.0. This variation can be attributed to the local changes of surface curvature. Figures 8(a) to (f) show that, for  $a/b$  of 2.0 and greater, the maximum Mach number occurs very near the inlet highlight ( $x = 0$ ). For  $a/b$  of 1.5 the maximum Mach number occurs approximately midway between the inlet highlight and throat (figs. 8(a), (b), (e), and (f)).

In order to determine an optimum  $a/b$  ratio, the average and local adverse Mach number gradients must be closely examined. Figures 8(a), (b), (e), and (f) indicate that the maximum average Mach number gradient from peak to throat occurs at an  $a/b$  ratio of 1.5. Relatively small differences exist in the average adverse Mach number gradient when comparing  $a/b$  ratios of 2.0 and greater. However, differences do exist in the distribution of the local Mach number gradients. The initial adverse local Mach number gradient just downstream of the inlet highlight is smallest at an  $a/b$  value of 2.0, and increases with increasing  $a/b$ . This result is especially evident at contraction ratios of 1.30 and 1.34 (figs. 8(a) to (d)). At the inlet throat location an  $a/b$  ratio of 3.0 has the smallest local Mach number gradient (figs. 8(c) and (d)). Since the boundary layer is less likely to separate on the inlet lip having the smallest initial local Mach number gradient, an  $a/b$  ratio of 2.0 may be near optimum.

The maximum Mach numbers from figure 8 are crossplotted as a function of major- to minor-axis ratio in figure 9. The minimum value of the maximum surface Mach number occurs at an  $a/b$  of approximately 2.0 for contraction ratios of 1.3 and 1.42.

The effect of major- to minor-axis ratio on the circumferential variation of maximum surface Mach number for each circumferential angle is illustrated in figure 10(a) for an incidence angle of  $30^\circ$  and free-stream velocity of 42.6 m/sec. The smallest circumferential variation in maximum surface Mach number occurs for an  $a/b$  of 2.0. The largest circumferential variation in maximum surface Mach number occurs at an  $a/b$  of 2.5. The circumferential variation of surface Mach number at the throat location is illustrated in figure 10(b). The larger the  $a/b$  ratio is, the greater the distance between the inlet highlight and the throat plane (fig. 3(b)). Thus, the largest  $a/b$  ratio (2.5) results in the smallest circumferential variation of surface Mach number at the inlet throat. There is a 35 percent increase in surface Mach number at the throat at  $\psi = 0^\circ$  as  $a/b$  is decreased from 2.5 to 1.5.

The largest  $a/b$  ratio results in the smallest variation in passage Mach number distribution at the throat location, as shown in figure 11. For static conditions (fig. 11(a)) the Mach number at the throat plane varies from 0.59 on the inlet centerline to 0.85 on the surface for an  $a/b$  of 2.5. However, for an  $a/b$  of 1.5, the Mach number varies from 0.55 on the inlet centerline to 1.1 on the surface. The effect of  $a/b$  is similar at an incidence angle of  $30^\circ$  (fig. 11(b)), where the Mach number distribution is skewed. These trends apply for all contraction ratios investigated.

In general, it is desirable to select an  $a/b$  ratio that minimizes the maximum surface Mach number, the average Mach number gradient (from peak to throat), and the local Mach number gradients on the lip surface. It is also desirable to minimize the circumferential and passage Mach number gradients in the throat plane since the throat is the inlet to the diffuser.

In summary, figures 8 to 11 show that for a given contraction ratio an  $a/b$  of 2.0 yields (1) the minimum peak Mach number and (2) the minimum local Mach number gradient on the lip surface. However, smaller circumferential and passage Mach number gradients at the throat were obtained for  $a/b$  greater than 2.0. Thus, a trade-off must be accepted between the effects of surface and passage Mach number distributions.

#### Effect of Internal Lip Super-Ellipse Exponent.

The effect of internal lip super-ellipse exponent  $n$  is presented in figure 12 for static conditions and for a free-stream velocity of 42.6 m/sec at  $30^\circ$  incidence angle. The effect of  $n$  on the lip geometry is illustrated in figure 2(c) for  $n$  ranging from 1.75 to 2.5. Figures 12(a) to (f) show that for  $n$  of 2.0 or less, the maximum Mach number occurs very near the inlet highlight. For  $n$  of 2.25 and 2.5, the maximum Mach number occurs downstream of the inlet highlight.

By examining the Mach number gradients of figures 12(a) to (d), it is observed that an  $n$  of 2.0 results in the minimum average Mach number gradient from peak to throat for an  $a/b$  of 2.0. However, for an  $a/b$  of 2.5 (figs. 12(e) and (f)), an  $n$  of 2.25 results in the minimum average Mach number gradient on the lip surface.

The maximum surface Mach numbers of figure 12 are crossplotted in figure 13 as a function of super-ellipse exponent. The minimum value of maximum surface Mach number occurs at an  $n$  of 2.0 for a  $a/b$  of 2.0 and at  $n$  of approximately 2.25 for an  $a/b$  of 2.5.

Generalizing the previous results, the larger the major- to minor-axis ratio  $a/b$ , the larger the value of  $n$  required to minimize the Mach number gradient and Mach number level on the surface of the inlet lip. This relationship indicates that an optimum value of  $n$  depends on the  $a/b$  ratio selected for a given application. For an  $a/b$  of 2.0, the optimum value of  $n$  corresponds to 2.0. However, when small flow Mach number gradients are required in the throat, an  $a/b$  ratio of 2.5 may be desired, which corresponds to an optimum value of  $n$  of approximately 2.25. These results apply to the 1.30 and 1.34 contraction ratio inlets.

## Effect of External Forebody Geometry

The previous discussion considered the effects of the internal lip geometric variables on the low-speed characteristics of the inlet. Considered next are the effects of the external forebody shape (fig. 3) on both the low-speed and cruise characteristics of the inlet. The external forebody geometries were obtained by varying the super-ellipse exponent  $m$  and by changing the diameter ratio  $D_1/D_{\max}$ . The degree of bluntness of the external forebody increases as  $m$  increases from 1.78 (approximate NACA-1 contour) to 2.15 (fig. 3).

Low-speed operation. - The effect of external forebody geometry on the surface Mach number distribution is presented in figure 14 for both the static condition and a free-stream velocity of 42.6 m/sec. Increasing  $m$  from 1.78 to 2.15 results in a slight reduction of Mach number near the inlet highlight for static conditions (figs. 14(a) and (c)). For a free-stream velocity of 42.6 m/sec and an incidence angle of  $30^\circ$  (fig. 14(b)), there is a negligible decrease in the Mach number near the inlet highlight for a contraction ratio of 1.30. However, for a 1.42 contraction ratio (fig. 14(d)), there is a slight reduction in the peak Mach number as  $m$  is increased from 1.78 to 2.15. The effect of blunting is greatest at the higher contraction ratio because increasing the contraction ratio results in a sharper external forebody geometry (fig. 3). The effect of blunting the external forebody is most evident at an incidence angle of  $50^\circ$  (fig. 14(e)). The average Mach number gradient (from peak to throat) is reduced as the super-ellipse exponent is increased from 1.78 to 1.95.

Cruise operation. - According to the previous results, low-speed inlet performance may be improved by increasing the contraction ratio and by blunting the external forebody. However, the effect of any changes in inlet geometry must also be evaluated at cruise conditions. Two important parameters affecting cruise performance are the mass flow ratio  $A_0/A_1$  and the diameter ratio  $D_1/D_{\max}$ . Along with the external forebody shape, they determine the cruise drag characteristics of the inlet cowl. Shown in figure 15 is a schematic of a typical flow field encountered at subsonic cruise. The mass flow ratio is an indication of how much airflow is spilled around the highlight. The diameter ratio  $D_1/D_{\max}$  is a measure of the external forebody frontal area available to turn the spilled air back to the axial direction. If the spilled flow is not efficiently turned, lip suction will not cancel the additive drag and a retarding force will be exerted on the nacelle. Experience has shown that, as spillage increases (decreasing  $A_0/A_1$ ) beyond a limiting value, the external forebody frontal area must also increase (decreasing  $D_1/D_{\max}$ ) to avoid drag penalties. To examine the effect of inlet geometry on cruise performance, some assumptions were made about the overall inlet geometry. Recall that for the present study the ratio of external forebody length to maximum nacelle diameter was fixed at an  $L/D_{\max}$  of 0.375 (fig. 1). Also fixed was the ratio of throat diameter to maximum nacelle diameter, at  $D_T/D_{\max} = 0.731$ . These assumptions were

made to simplify the task of systematically varying inlet geometry for low-speed performance. However, as can be deduced from reference 2, these assumptions will not result in an optimum inlet design at cruise for all mass flow ratios. The resulting inlet geometries do, however, allow some general conclusions to be drawn about inlet performance at cruise speed.

With the previous assumptions, inlet highlight to maximum diameter ratio can be written in terms of contraction ratio as follows:

$$\text{Contraction ratio} = \frac{A_1}{A_T} = \left(\frac{D_1}{D_T}\right)^2 \quad (3)$$

$$\text{Diameter ratio} = \frac{D_1}{D_{\max}} = \left(\frac{D_1}{D_T}\right)\left(\frac{D_T}{D_{\max}}\right) \quad (4)$$

Therefore, for the present inlet geometry,

$$\frac{D_1}{D_{\max}} = \left(\frac{A_1}{A_T}\right)^{1/2} \quad (0.731) \quad (5)$$

As contraction ratio increases, external forebody diameter ratio must also increase. The table on figure 15 shows the resulting relationship between contraction ratio and diameter ratio for the present inlets. This relationship is valid only for the previously mentioned assumption of constant  $D_T/D_{\max}$  and is intended to illustrate the general effect of increasing contraction ratio.

The effect of diameter ratio and mass flow ratio on the maximum external surface Mach number is presented in figure 16 at a free-stream Mach number of 0.80 and at zero incidence angle. The external forebody is an NACA-1 series shape. Mach number curves of constant mass flow  $A_0/A_1$  ranging from 0.55 to 0.70 are shown. The mass flow ratio was changed by varying the weight flow through the inlet. The resulting one-dimensional throat Mach numbers are indicated on the figure. Contraction ratio is indicated along the bottom of the figure. High values of surface Mach number are to be avoided in order to minimize strong shocks on the external forebody and to obtain efficient turning of the spilled flow. The figure clearly shows that the lowest surface Mach numbers are obtained at the highest mass flow ratio and lowest diameter ratio. This result is not surprising since these conditions result in minimum spillage with maximum external forebody frontal area available for turning of the spilled flow. The figure shows that increasing contraction ratio will result in higher external forebody surface Mach numbers at cruise, and hence generally poorer cruise performance. The diameter ratio could have, of course, been held constant with increasing contraction ratio by either

reducing the throat diameter, and therefore increasing the throat Mach number, or by increasing the maximum nacelle diameter (see eqs. (3), (4), and (5)). In general, however, both these alternatives will cause penalties in nacelle aerodynamic performance and weight.

As shown in figure 3, the shape of the external forebody was blunted by increasing the exponent  $m$  of the super-ellipse curve used to generate the surface from 1.78 (approximate NACA-1 series shape) to 1.95 and 2.15. Blunting has the effect of reducing the curvature near the highlight. This same effect could have been obtained by reducing the length  $L$  of the external forebody. The effect of this blunting on the external forebody maximum surface Mach number is shown in figure 17 as a function of mass flow ratio. One-dimensional throat Mach number is shown along the bottom of the figure. Figure 17(a) indicates that, for a diameter ratio of 0.833, blunting the external forebody contour (or reducing the external forebody length below  $L = 0.375 D_{\max}$ ) will increase the surface Mach number and possibly lead to increased cruise drag. Figure 17(b) shows that quite different results were obtained at a diameter ratio of 0.871. Here blunting reduced the maximum surface Mach number at a mass flow ratio of 0.55. At mass flow ratios above approximately 0.6 a minimum surface Mach number is obtained at some degree of bluntness between the extremes considered. This figure indicates that, in terms of surface Mach number, there exists an optimum external forebody bluntness or length. This result is consistent with the empirically and analytically derived external forebody design charts of reference 2. These charts show that the selection of the external forebody length is indeed a function of both mass flow ratio and diameter ratio.

Figures 16 and 17 illustrate analytically the well-known fact that complex trade-offs are required between the inlet geometries that give good low-speed performance and those desired at cruise. An investigation of these trade-offs is beyond the scope of this report.

## SUMMARY OF RESULTS

The effect of subsonic inlet lip geometry on predicted surface and passage Mach number distributions is illustrated. The theoretical results were obtained from incompressible potential flow calculations corrected for compressibility. The major emphasis of this investigation was on the low-speed (takeoff and landing) operating conditions. The low-speed results were obtained for three geometric variables of interest. They are the contraction ratio  $A_1/A_T$ , defined as the ratio of highlight area to throat area; the internal lip major- to minor-axis ratio  $a/b$ ; and the internal lip super-ellipse exponent  $n$ . This report investigated the following range of these variables:  $A_1/A_T$ , 1.3 to 1.42;  $a/b$ , 1.5 to 3.0;  $n$ , 1.75 to 2.5. The low-speed results were obtained at both static conditions and a free-stream velocity of 42.6 m/sec, with incidence angles ranging from  $0^\circ$  to  $50^\circ$ . The effect of inlet diameter ratio and blunting the external forebody on max-

imum external surface Mach number was illustrated at a cruise Mach number of 0.8. The principal results of this study are as follows:

1. Of the three geometric variables considered, contraction ratio had the largest effect on the Mach number distribution. The effect of contraction ratio on surface Mach number was greatest at the high incidence angles on the windward side of the inlet. At an incidence angle of  $40^\circ$ , there was a 27 percent reduction in maximum surface Mach number as contraction ratio was increased from 1.3 to 1.42. The maximum surface Mach number and the average surface Mach number gradient from peak to throat were lowest for the highest-contraction-ratio inlet (1.42) investigated. There was little difference in the maximum local surface Mach number gradient that occurred at the throat location for all contraction ratios. The inlet with the lowest contraction ratio (also having the shortest lip) had the largest circumferential variation in surface Mach number and the largest passage Mach number gradient at the throat plane.

2. For a given contraction ratio, the peak Mach number and the initial local Mach number gradient just downstream of the inlet highlight was smallest at an  $a/b$  of 2.0 and increased with increasing  $a/b$ . Smaller circumferential and passage Mach number gradients were obtained at the throat plane with  $a/b$  greater than 2.0. Thus, a trade-off must be accepted between the effects of surface Mach number on the entry lip and passage Mach number distributions at the throat plane.

3. In general, the larger the major- to minor-axis ratio, the larger the value of the internal super-ellipse exponent  $n$  required to minimize the Mach number gradient and Mach number level on the lip surface. For an  $a/b$  of 2.0, the optimum value of  $n$  corresponded to 2.0. For an  $a/b$  of 2.5, the optimum value of  $n$  was approximately 2.25.

4. The inlet maximum surface Mach number at low speeds can be reduced by blunting the external forebody geometry. The effect of blunting was greatest at high incidence angles and at high contraction ratios. Any change made in inlet geometry to improve the low-speed operation must also be evaluated at cruise.

5. The lowest maximum external surface Mach numbers at cruise ( $M_0 = 0.8$ ) were obtained at the highest mass flow ratio and lowest highlight to maximum diameter ratio. The effect of blunting the external forebody geometry on cruise performance is a function of mass flow ratio and diameter ratio. For a diameter ratio of 0.833, blunting the external forebody increased the maximum surface Mach number at all mass flow ratios. However, for a diameter ratio of 0.871, blunting the external forebody reduced the maximum surface Mach number for mass flow ratios below 0.6.

Lewis Research Center

National Aeronautics and Space Administration,  
Cleveland, Ohio, August 7, 1973,  
501-24.

## APPENDIX A

### SYMBOLS

A	area
$A_1/A_T$	inlet contraction ratio (fig. 15)
$A_0/A_1$	mass flow ratio (fig. 15)
a	major axis of internal lip geometry (fig. 1)
b	minor axis of internal lip geometry (fig. 1)
D	diameter
L	external forebody length (fig. 1)
M	Mach number
$\bar{M}$	one-dimensional Mach number at throat plane
m	external forebody super-ellipse exponent
N	a normal to the body surface
n	internal lip super-ellipse exponent
p, q	arbitrary points on inlet surface (fig. 19)
R	distance between two source points (fig. 19)
r	radius from inlet axis
S	surface area
s	local surface distance from stagnation point
$s_{max}$	surface distance between stagnation point and reference plane (fig. 1)
V	velocity
W	axial distance from inlet highlight to reference plane (fig. 1)
x	axial distance from inlet highlight (fig. 1)
Y	external forebody thickness
y	radial distance from highlight
$\alpha$	incidence angle of inlet, angle between free-stream velocity and inlet axis (fig. 1)
$\rho$	density

$\sigma$  source intensity on surface element  
 $\psi$  circumferential angle around inlet (fig. 1)

Subscripts:

c compressible  
i incompressible  
max maximum  
s surface  
T throat  
0 free stream  
1 highlight  
I, II, III basic potential flow solutions for inlet

Superscript:

( $\rightarrow$ ) vector

## APPENDIX B

### METHOD OF SOLUTION

The theoretical Mach number distributions were obtained by use of three computer programs presented schematically in figure 18. The first program, SCIRCL, uses a super-ellipse to represent the surface and to generate a coordinate point spacing for the second program. The second program, EOD, is the Douglas axisymmetric incompressible potential flow program. The method (ref. 6) utilizes a large number of sources and sinks distributed on the surface of the inlet. It is assumed that each surface element is a straight line segment and that the source or sink is located at the midpoint of each element (fig. 19). The central problem of the Douglas analysis is the solution of the integral equation

$$2\pi\sigma(p) - \int_S \frac{\partial}{\partial N} \left[ \frac{1}{R(p,q)} \right] \sigma(q) dS = -\vec{V}_0 \cdot \vec{N} \quad (B1)$$

where  $\sigma$  is the unknown source intensity on each surface element. The first term of equation (B1) is the normal velocity induced at  $p$  by a source at  $p$ . The second term is the combined effect of the sources at other points  $q$  on the surface of the body  $S$ . The quantity

$$\frac{\partial}{\partial N} \left[ \frac{1}{R(p,q)} \right]$$

depends only on the geometry of the surface. The term on the right side of equation (B1) is the normal component of the free-stream velocity at  $p$ . The integral equation (B1) is solved by approximating it by a set of linear algebraic equations. The velocities on and off of the body surface are calculated from the source distribution.

The EOD program is used to obtain three basic solutions for flow around inlets (fig. 20). These solutions provide a convenient basis for generating the combined solution that is of prime interest. The three basic solutions are  $V_I$ , axial flow with the inlet duct extension closed;  $V_{II}$ , axial flow with the duct open; and  $V_{III}$ , the crossflow solution with the duct extension open. These solutions are used as an input to a third computer program, called COMBYN. This program combines the three basic solutions to obtain a solution for any combination of free-stream velocity, inlet incidence angle, and mass flow rate through the inlet. Then the combined solution  $\vec{V}$  can be expressed as

$$\vec{V} = A\vec{V}_I + B\vec{V}_{II} + C\vec{V}_{III} \quad (B2)$$

where A, B, and C are the combination coefficients and are discussed in detail in reference 5. The program COMBYN also corrects the internal incompressible potential flow solution for compressibility by using the method of reference 7. This reference proposed the following relation between the local incompressible velocity  $V_i$  and the local compressible velocity  $V_c$ ,

$$V_c = V_i \left( \frac{\rho_i}{\bar{\rho}_c} \right)^{V_i/\bar{V}_i} \quad (B3)$$

where

- $\rho_i$             incompressible density equal to compressible stagnation density
- $\bar{\rho}_c$             average compressible density across flow passage
- $\bar{V}_i$             average incompressible velocity across flow passage at given station

Since equation (B3) was derived for internal flow solutions, it was modified to correct the external surface Mach numbers at cruise conditions as follows:

$$V_c = V_i \left( \frac{\rho_i}{\rho_0} \right)^{V_i/V_0} \quad (B4)$$

where  $V_0$  is the free-stream velocity at cruise conditions and  $\rho_0$  is the free-stream density. This expression compares favorably with the Gothert compressibility correction (ref. 8) and is more convenient to use.

## REFERENCES

1. Albers, James A. : Predicted Upwash Angles at Engine Inlets for STOL Aircraft. NASA TM X-2593, 1972.
2. Hancock, J. P. ; and Hinson, B. L. : Inlet Development for the L-500. Paper 69-448, AIAA, June 1969.
3. Albers, James A. : Theoretical and Experimental Internal Flow Characteristics of a 13.97-Centimeter-Diameter Inlet at STOL Takeoff and Approach Conditions. NASA TN D-7185, 1973.
4. Miller, Brent A. ; and Abbott, John M. : Low-Speed Wind-Tunnel Investigation of the Aerodynamic and Acoustic Performance of a Translating-Centerbody Choked-Flow Inlet. NASA TM X-2773, 1973.
5. Stockman, Norbert O. : Potential Flow Solutions for Inlets of VTOL Lift Fans and Engines. Analytic Methods in Aircraft Aerodynamics. NASA SP-228, 1970, pp. 659-681.
6. Hess, J. L. ; and Smith, A. M. O. : Calculation of Potential Flow About Arbitrary Bodies. Progress in Aeronautical Sciences. Vol. 8. D. Küchemann, ed. , Pergamon Press, 1967, pp. 1-138.
7. Lieblein, S. ; and Stockman, N. O. : Compressibility Correction for Internal Flow Solutions. J. Aircraft, vol. 9, no. 4, Apr. 1972, pp. 312-313.
8. Shapiro, Ascher H. : The Dynamics and Thermodynamics of Compressible Fluid Flow. Vol. I. Ronald Press Co. , 1953, pp. 316-321.

TABLE I. - INLET GEOMETRIC VARIABLES CONSIDERED IN THIS INVESTIGATION

Contraction ratio, $A_1/A_T$	Major- to minor-axis ratio, a/b	Internal lip super-ellipse exponent, n	External forebody super-ellipse exponent, m	Ratio of highlight diameter to maximum diameter, $D_1/D_{max}$	Ratio of throat diameter to maximum diameter, $D_T/D_{max}$	Ratio of external forebody length to maximum diameter, $L/D_{max}$
1.30	2.0	2.0	NACA-1(1.78)	0.833	0.731	0.375
1.34	↓	↓	↓	.846	↓	↓
1.38	↓	↓	↓	.858	↓	↓
1.42	↓	↓	↓	.871	↓	↓
1.30	1.5	↓	↓	.833	↓	↓
1.30	2.5	↓	↓	.833	↓	↓
1.34	2.5	↓	↓	.846	↓	↓
1.34	3.0	↓	↓	.846	↓	↓
1.42	1.5	↓	↓	.871	↓	↓
1.42	2.5	↓	↓	.871	↓	↓
1.30	2.0	1.75	↓	.833	↓	↓
1.30	↓	2.25	↓	.833	↓	↓
1.30	↓	2.50	↓	.833	↓	↓
1.34	↓	2.25	↓	.846	↓	↓
1.34	↓	2.50	↓	.846	↓	↓
1.30	2.5	2.25	↓	.833	↓	↓
↓	2.5	2.50	↓	↓	↓	↓
↓	2.0	2.0	Blunt(1.95)	↓	↓	↓
1.42	↓	↓	Blunt(2.15)	.871	↓	↓
1.42	↓	↓	Blunt(1.95)	.871	↓	↓
			Blunt(2.15)	.871	↓	↓

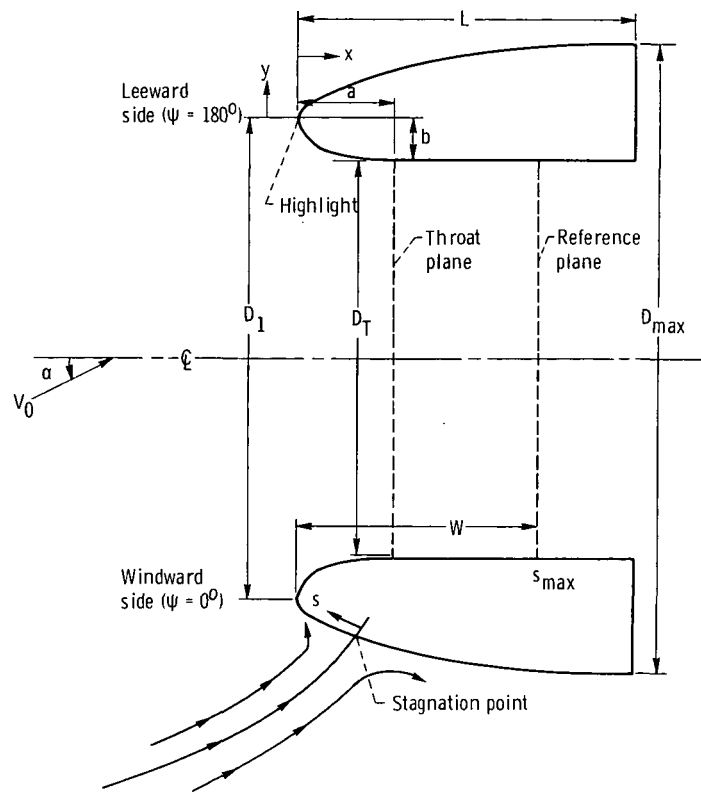
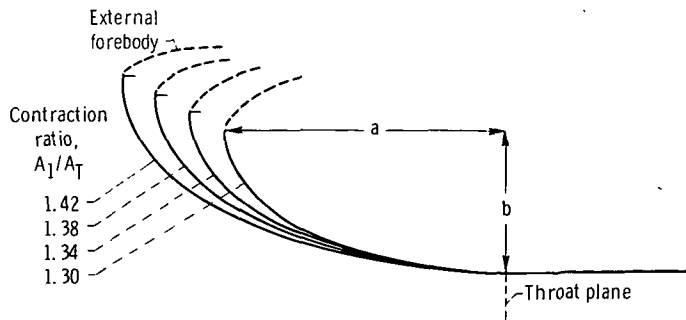
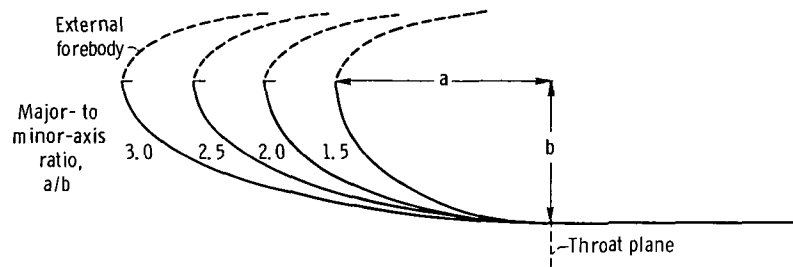


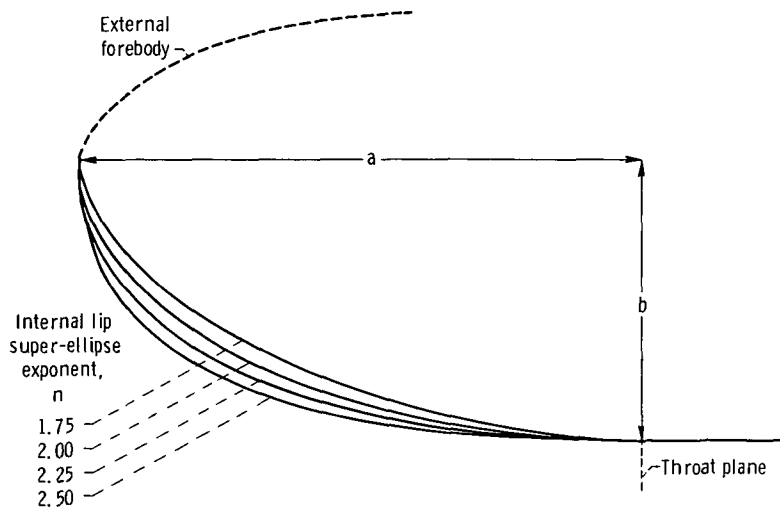
Figure 1. - Illustration of inlet geometric variables. Nondimensional ratios: throat diameter to maximum diameter,  $D_T/D_{max}$ , 0.731; length to maximum diameter,  $L/D_{max}$ , 0.375; distance between highlight and reference plane to maximum diameter,  $W/D_{max}$ , 0.278.



(a) Contraction ratio,  $A_1/A_T$ . Major- to minor-axis ratio,  $a/b$ , 2.0; super-ellipse exponent,  $n$ , 2.0.



(b) Major- to minor-axis ratio,  $a/b$ . Contraction ratio,  $A_1/A_T$ , 1.3; super-ellipse exponent,  $n$ , 2.0.



(c) Super-ellipse exponent,  $n$ . Contraction ratio,  $A_1/A_T$ , 1.3; major- to minor-axis ratio,  $a/b$ , 2.0.

Figure 2. - Illustration of internal lip geometric variables.

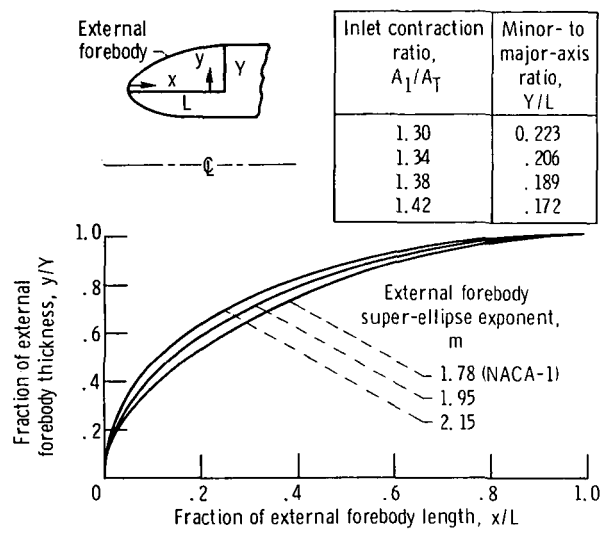


Figure 3. - Comparison of three external forebody shapes investigated. Forebody length  $L$  is constant.

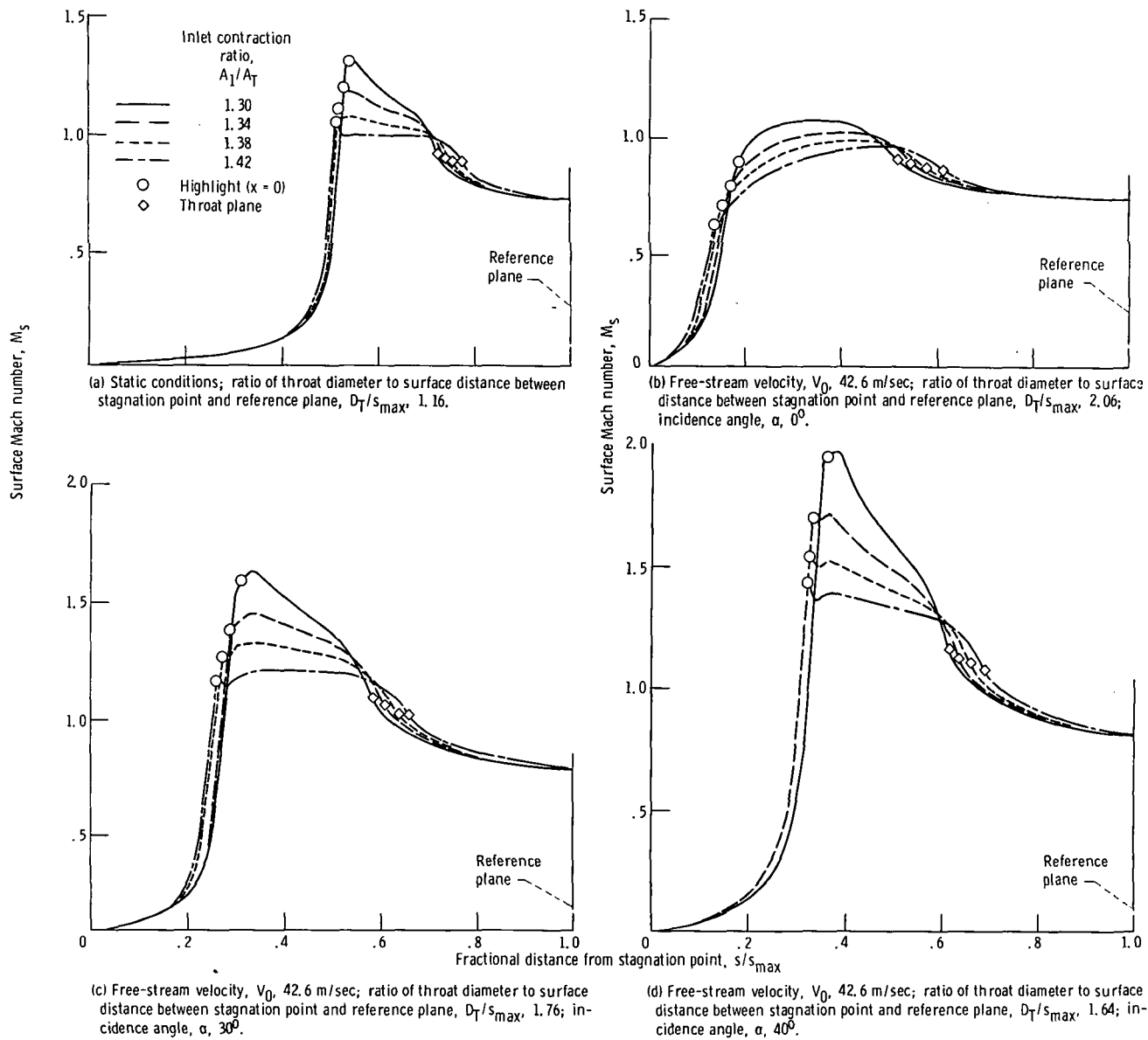


Figure 4. - Effect of inlet contraction ratio on surface Mach number distribution. Major- to minor-axis ratio,  $a/b$ , 2.0; internal lip super-ellipse exponent,  $n$ , 2.0; external forebody, NACA-1; circumferential angle,  $\psi$ ,  $0^\circ$ ; one-dimensional throat Mach number,  $M$ , 0.71.

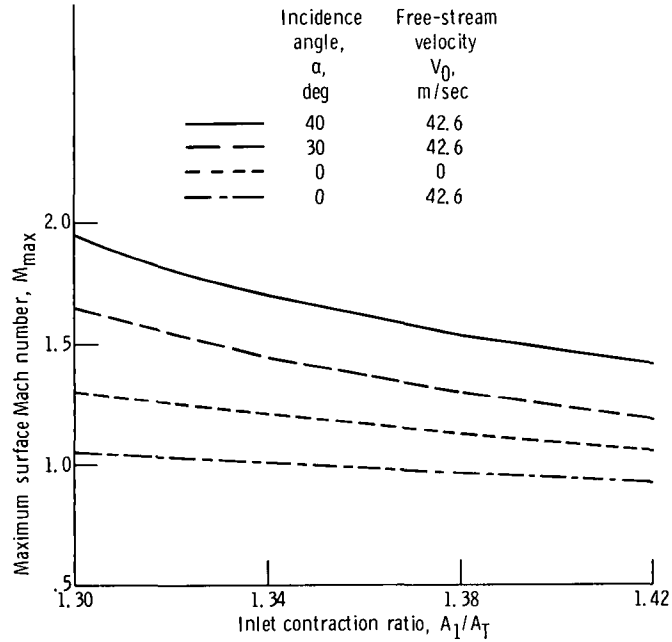


Figure 5. - Effect of inlet contraction ratio on maximum surface Mach number. Major- to minor-axis ratio,  $a/b$ , 2.0; internal lip super-ellipse exponent,  $n$ , 2.0; external forebody, NACA-1; circumferential angle,  $\psi$ ,  $0^\circ$ ; one-dimensional throat Mach number,  $\bar{M}$ , 0.71.

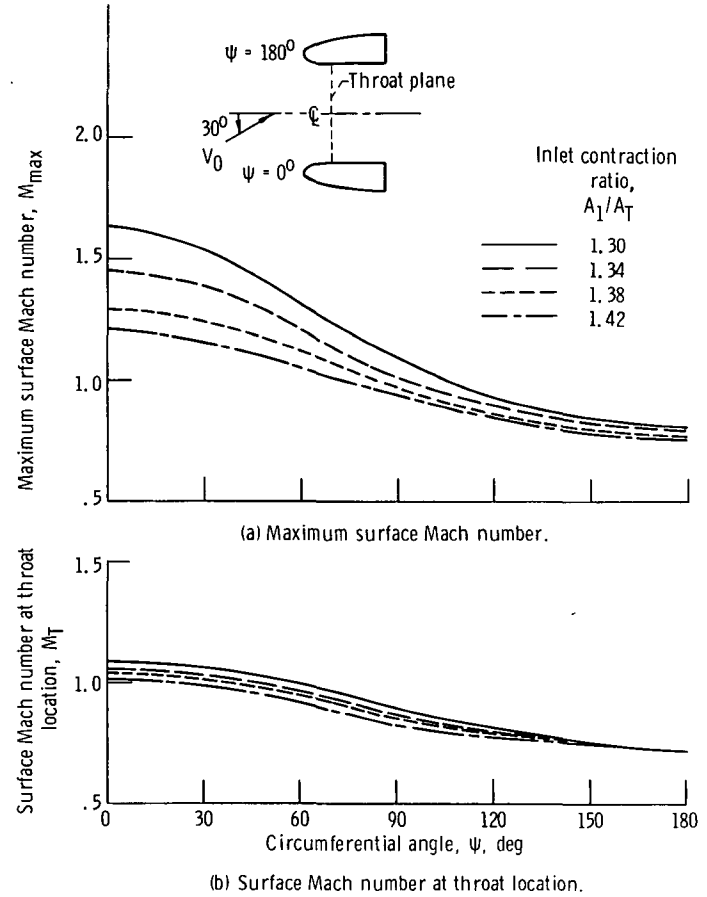
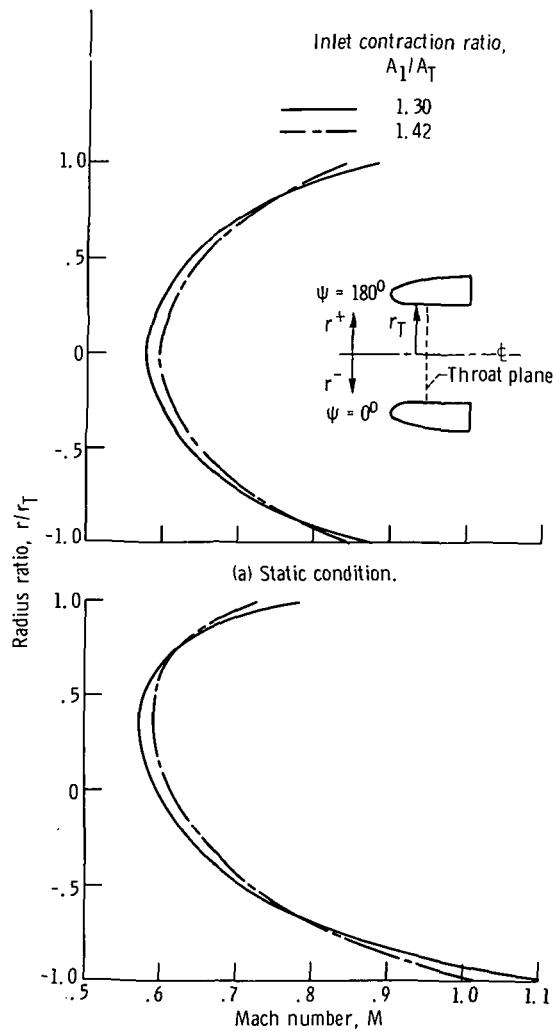


Figure 6. - Effect of inlet contraction ratio on circumferential variation of surface Mach number. Major- to minor-axis ratio,  $a/b$ , 2.0; internal lip super-ellipse exponent,  $n$ , 2.0; external forebody, NACA-1; incidence angle,  $\alpha$ ,  $30^\circ$ ; one-dimensional throat Mach number,  $\bar{M}$ , 0.71; free-stream velocity,  $V_0$ , 42.6 m/sec.



(b) Free-stream velocity,  $V_0$ , 42.6 m/sec; incidence angle,  $\alpha$ ,  $30^\circ$ .

Figure 7. - Effect of contraction ratio on radial distribution of Mach number at throat location. Major- to minor-axis ratio,  $a/b$ , 2.0; internal lip super-ellipse exponent,  $n$ , 2.0; external forebody, NACA-1; one-dimensional throat Mach number,  $M$ , 0.71.

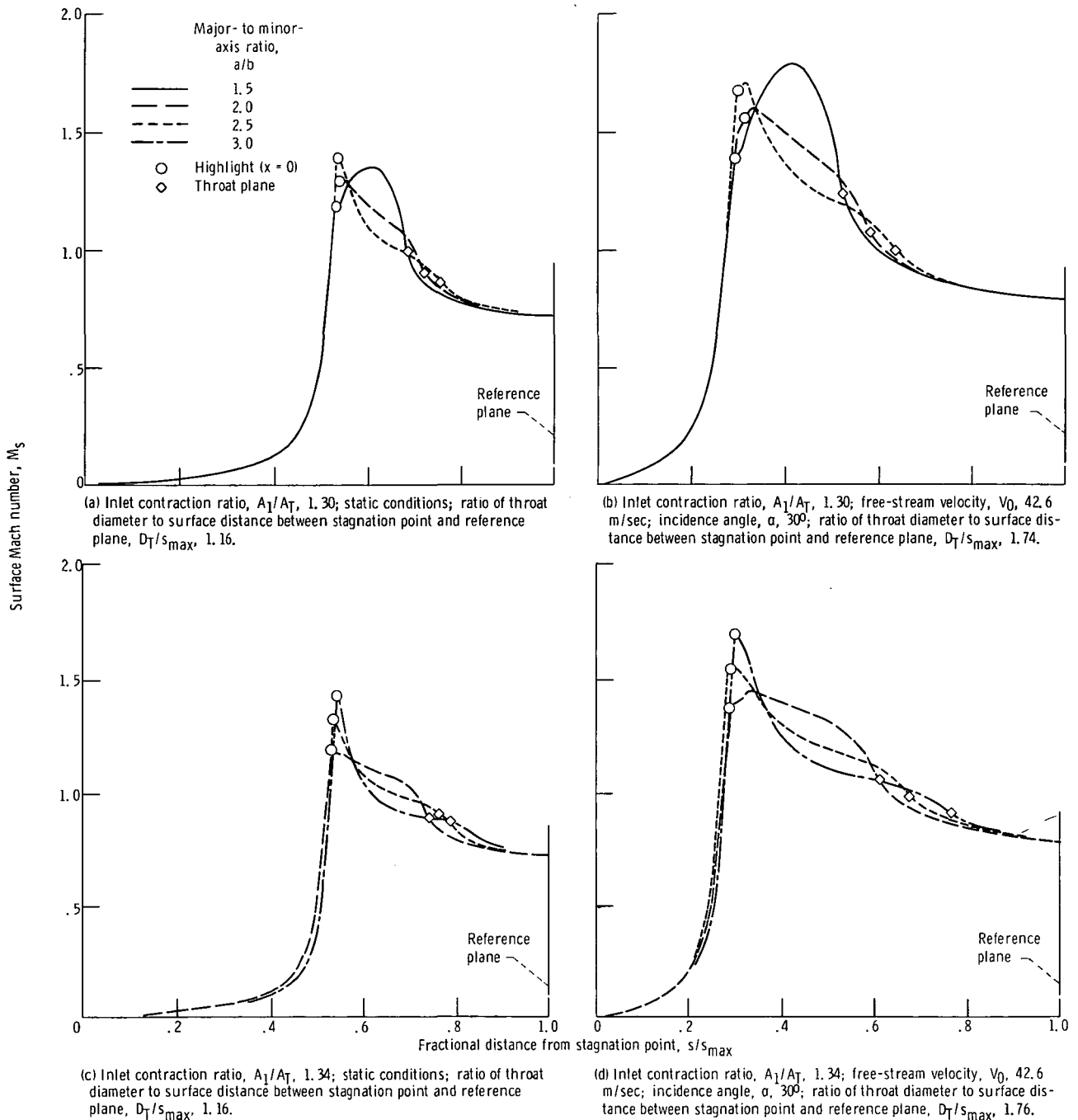
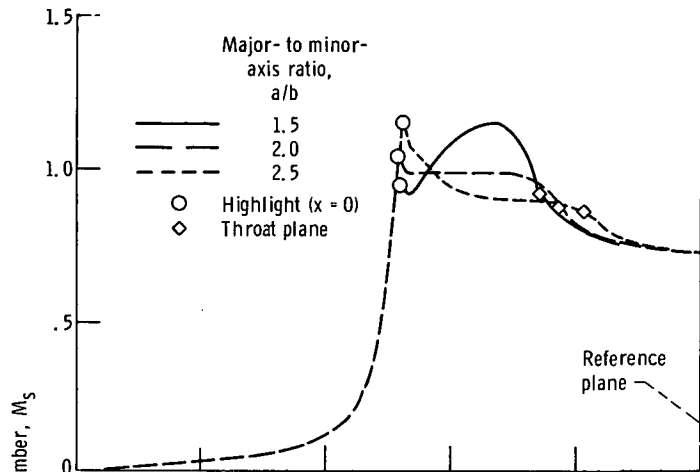
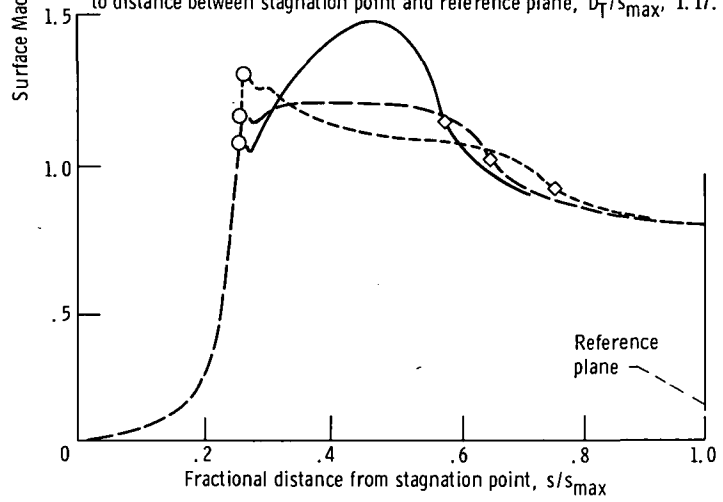


Figure 8. - Effect of major- to minor-axis ratio on surface Mach number distribution. Internal lip super-ellipse exponent,  $n$ , 2.0; external forebody, NACA-1; circumferential angle,  $\psi$ ,  $0^\circ$ ; one-dimensional throat Mach number,  $\bar{M}$ , 0.71.



(e) Inlet contraction ratio, 1.42; static condition; ratio of throat diameter to distance between stagnation point and reference plane,  $D_T/s_{max}$ , 1.17.



(f) Inlet contraction ratio,  $A_1/A_T$ , 1.42; free-stream velocity,  $V_0$ , 42.6 m/sec; incidence angle,  $\alpha$ ,  $30^\circ$ ; ratio of throat diameter to distance between stagnation point and reference plane,  $D_T/s_{max}$ , 1.78.

Figure 8. - Concluded.

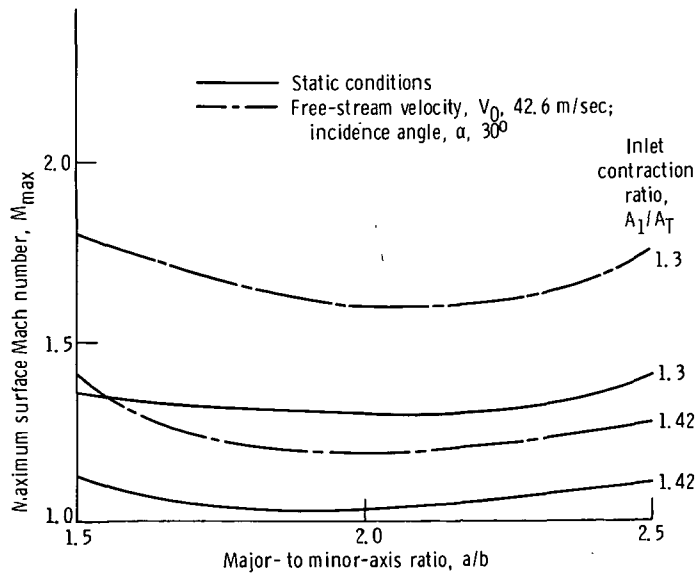


Figure 9. - Effect of major- to minor-axis ratio on maximum surface Mach number. Internal lip super-ellipse exponent,  $n$ , 2.0; external forebody, NACA-1; circumferential angle,  $\psi$ ,  $0^\circ$ ; one-dimensional throat Mach number,  $\bar{M}$ , 0.71.

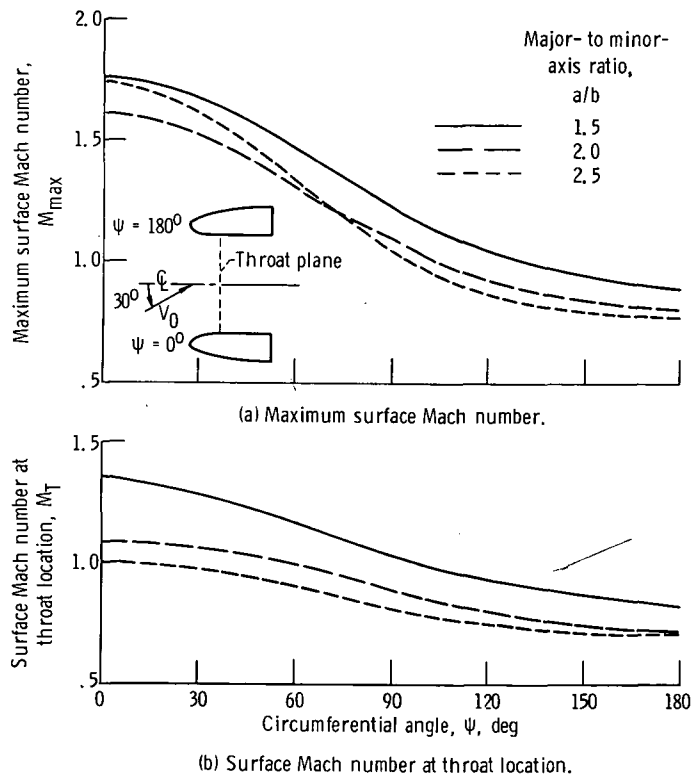


Figure 10. - Effect of major- to minor-axis ratio on circumferential variation of surface Mach number. Internal lip super-ellipse exponent,  $n$ , 2.0; inlet contraction ratio,  $A_1/A_T$ , 1.30; external forebody, NACA-1; incidence angle,  $\alpha$ ,  $30^\circ$ ; free-stream velocity,  $V_0$ , 42.6 m/sec; one-dimensional throat Mach number,  $\bar{M}$ , 0.71.

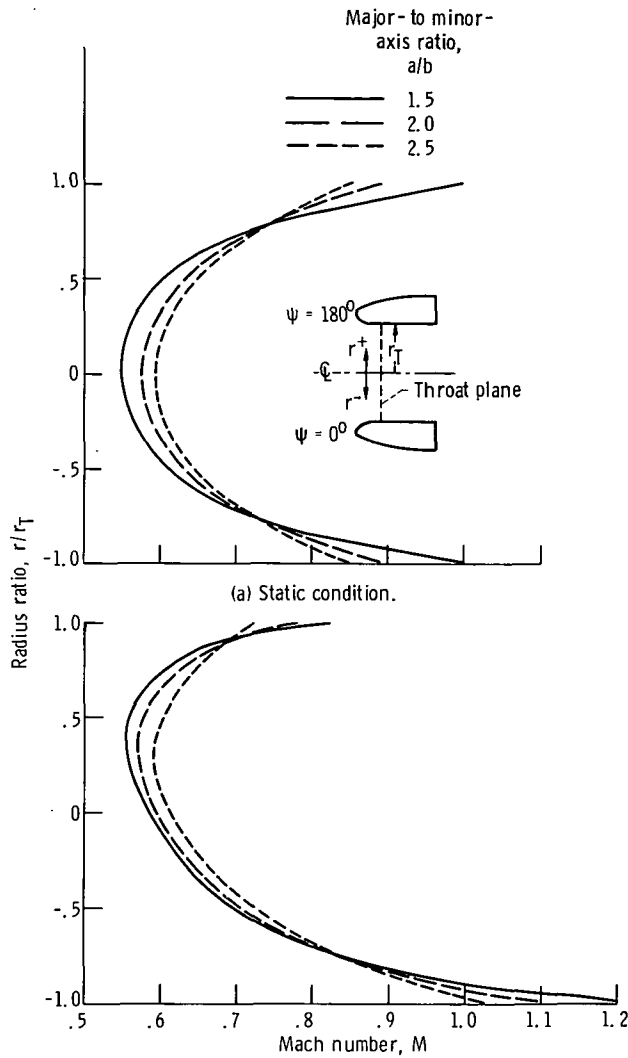


Figure 11. - Effect of major-to minor-axis ratio on radial distribution of Mach number at throat location. Internal lip superellipse exponent,  $n$ , 2.0; external forebody, NACA-1; inlet contraction ratio,  $A_1/A_T$ , 1.30; one-dimensional throat Mach number,  $\bar{M}$ , 0.71.

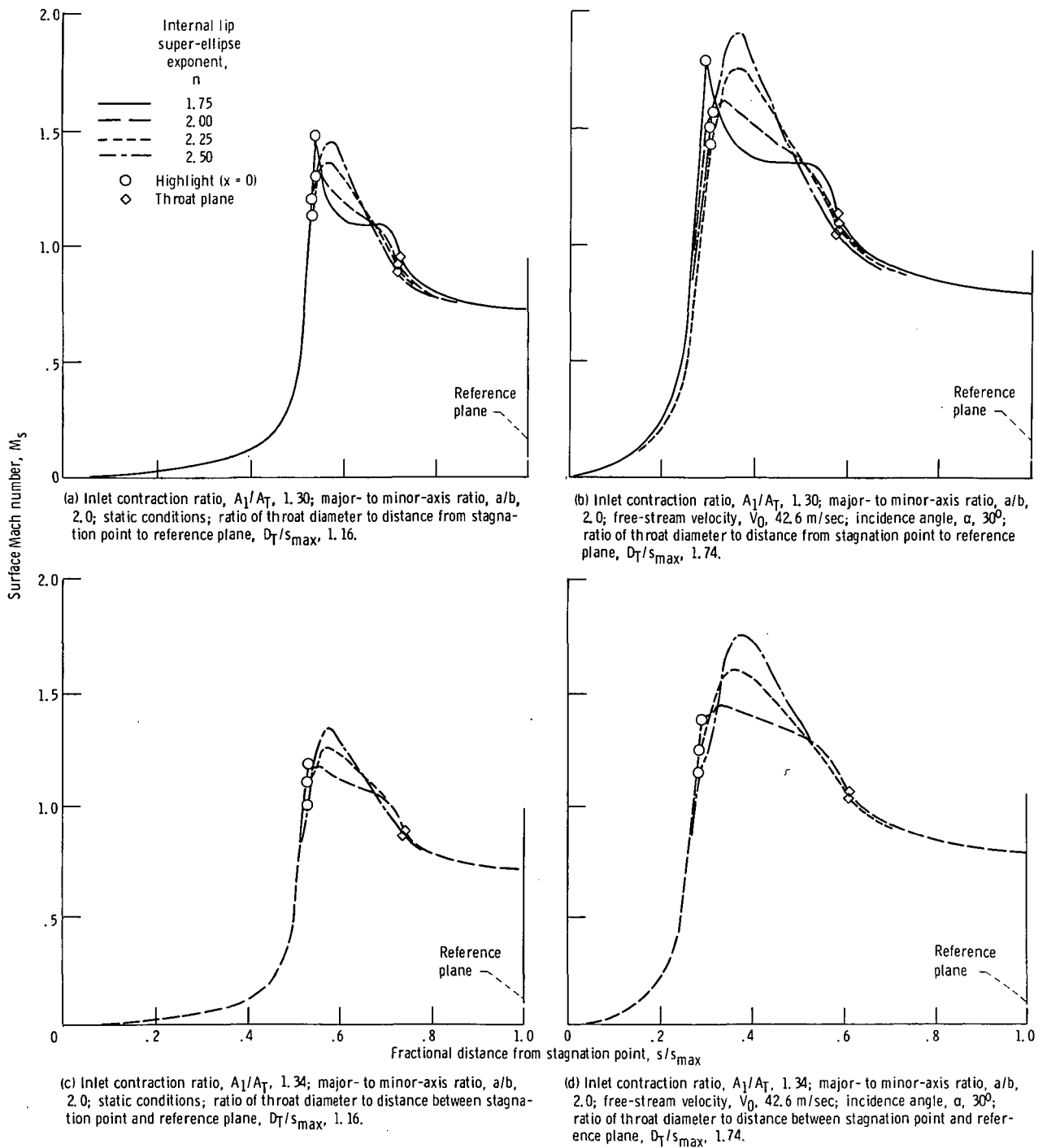


Figure 12. - Effect of internal lip super-ellipse exponent on surface Mach number distribution. External forebody, NACA-1; circumferential angle,  $\psi$ ,  $0^\circ$ ; one-dimensional throat Mach number,  $M$ , 0.71.

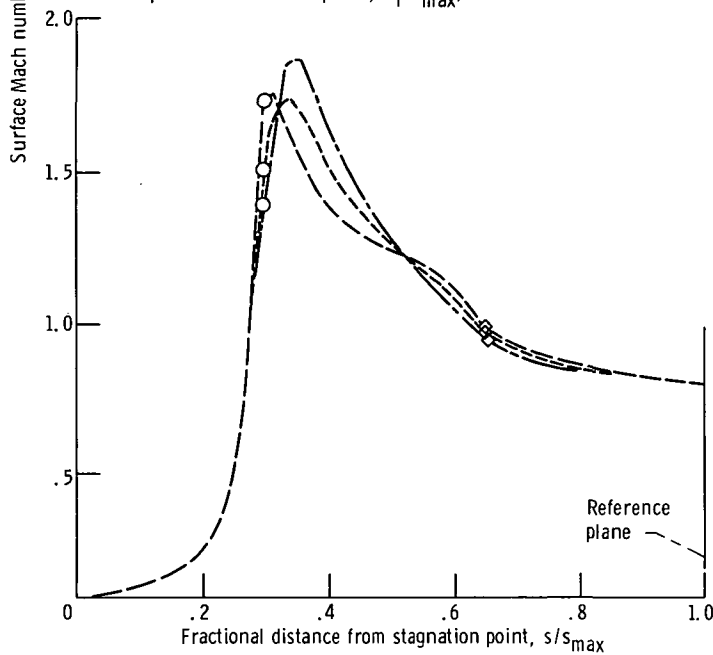
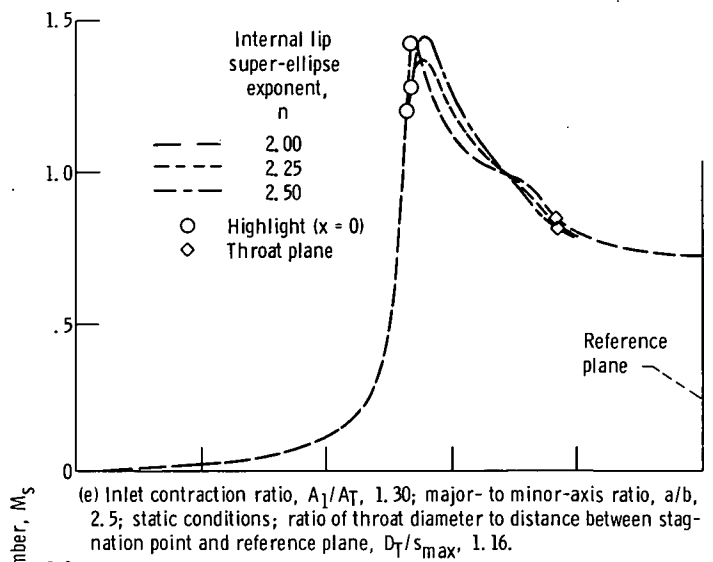


Figure 12. - Concluded.

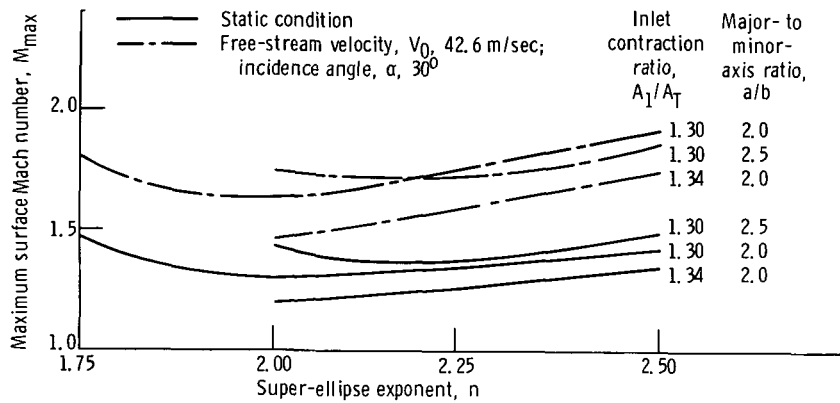


Figure 13. - Effect of super-ellipse exponent on maximum surface Mach number. External forebody, NACA-1; circumferential angle,  $\psi$ ,  $0^\circ$ ; one-dimensional throat Mach number,  $\bar{M}$ , 0.71.

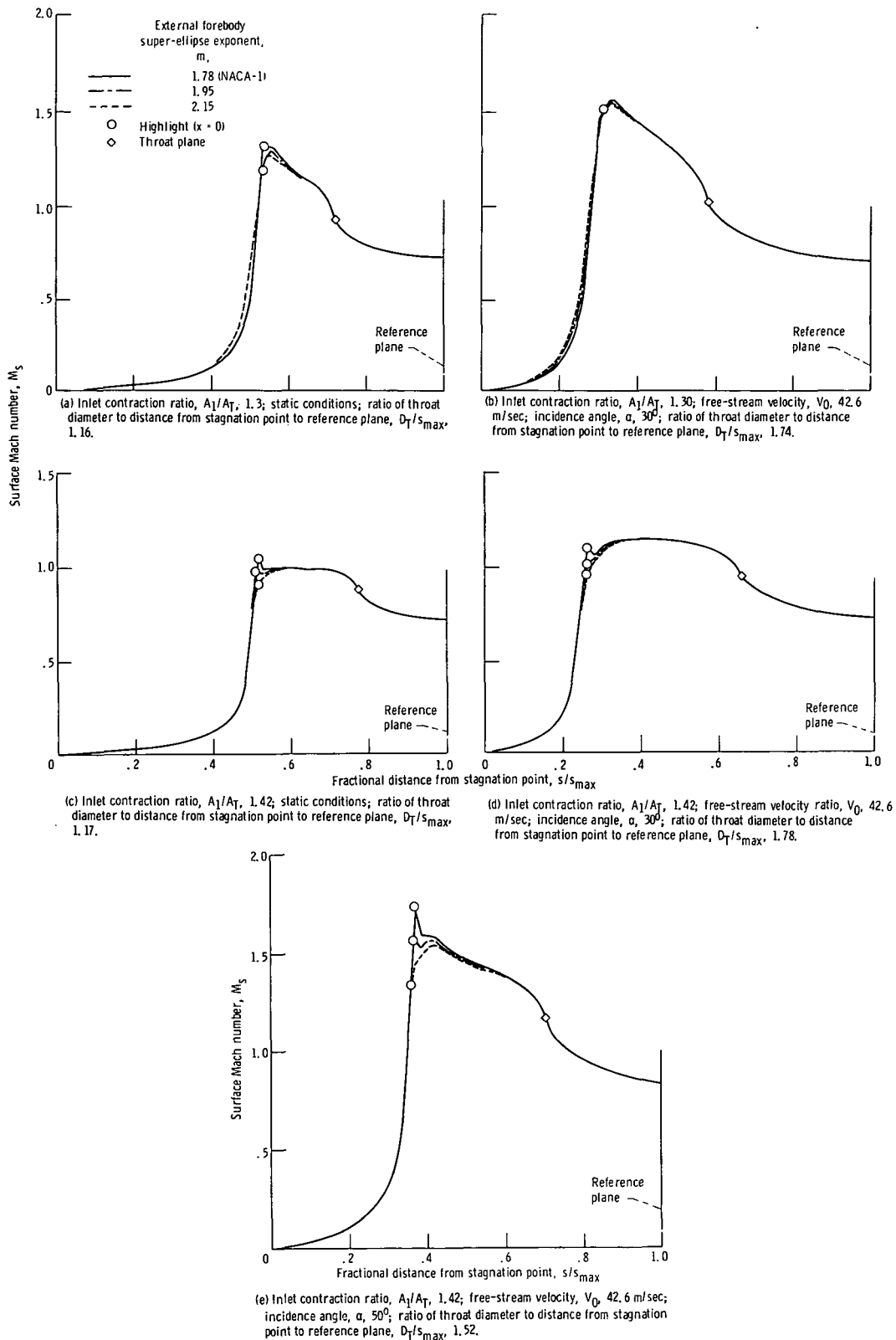


Figure 14. - Effect of external forebody on surface Mach number distribution. Major- to minor-axis ratio,  $a/b$ , 2.0; internal lip super-ellipse exponent,  $n$ , 2.0; circumferential angle,  $\psi$ ,  $0^\circ$ ; one-dimensional throat Mach number,  $\bar{M}$ , 0.71.

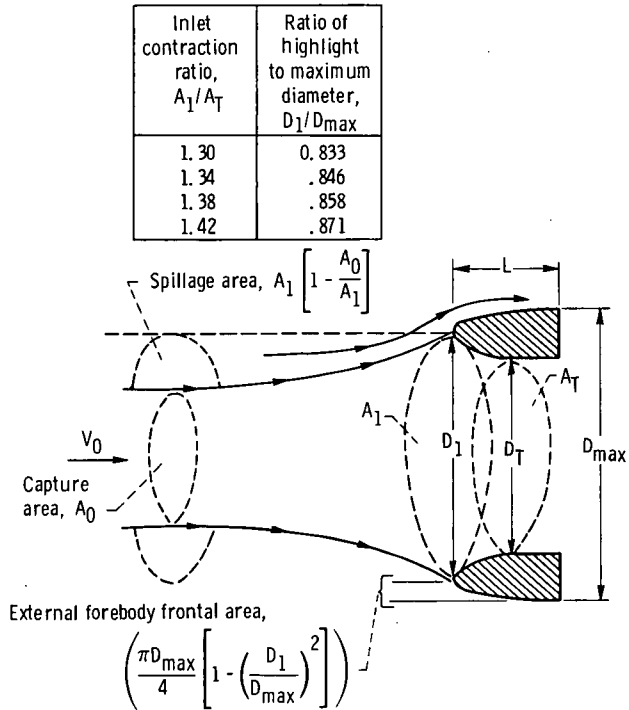


Figure 15. - Schematic of inlet flow at cruise conditions.

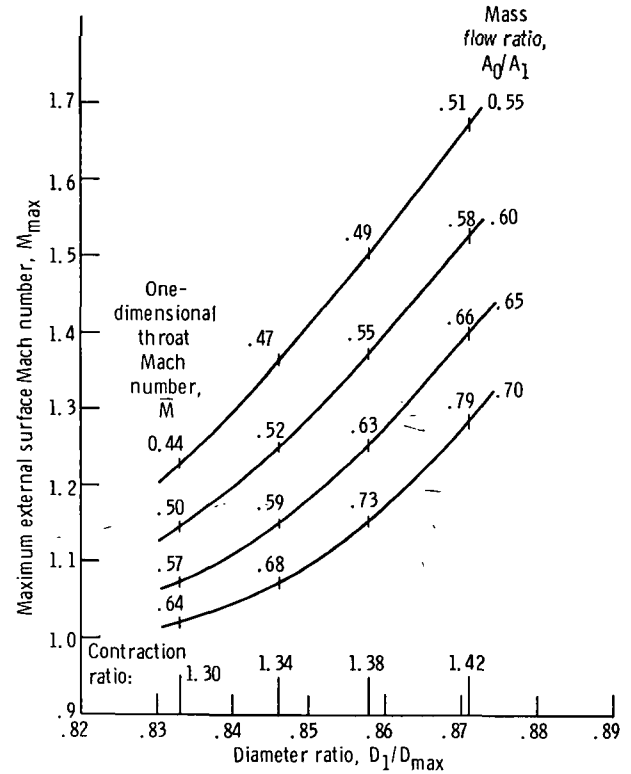


Figure 16. - Effect of diameter ratio on maximum external surface Mach number. External forebody, NACA-1; free-stream Mach number,  $M_0$ , 0.8; incidence angle,  $\alpha$ ,  $0^\circ$ .

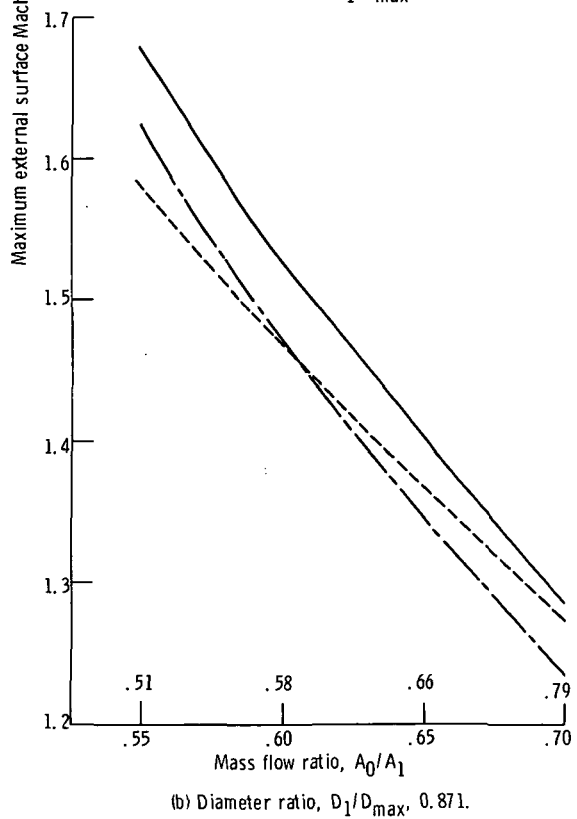
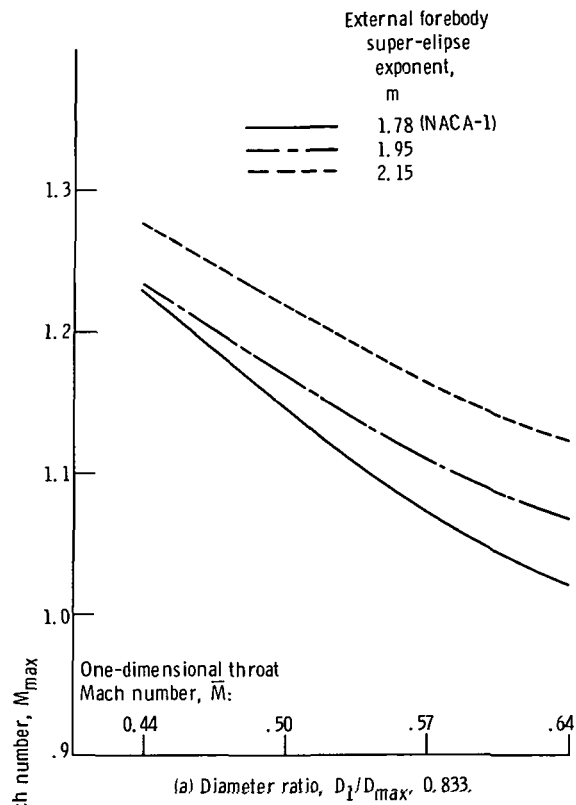


Figure 17. - Effect of mass flow ratio and external forebody shape on maximum external surface Mach number. Free-stream Mach number,  $M_0$ , 0.8; incidence angle,  $\alpha$ ,  $0^\circ$ .

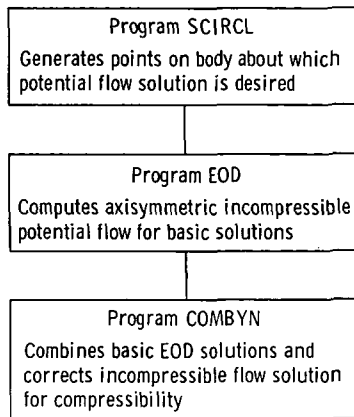


Figure 18. - Schematic representation of computer programs.

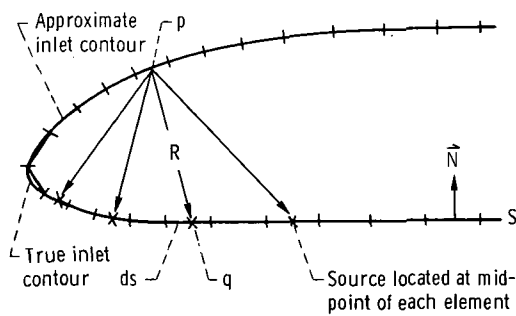
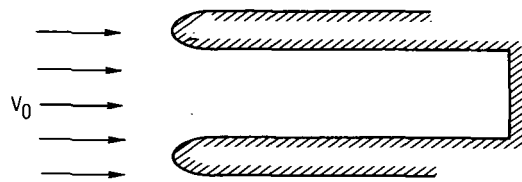
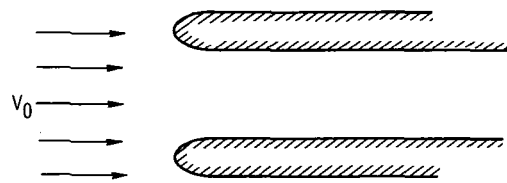


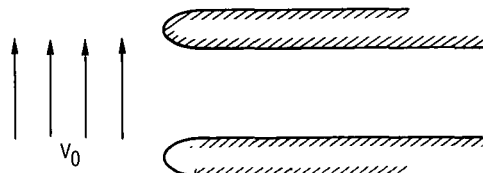
Figure 19. - Straight-line-element approximation to inlet surface.



(a) Axial-flow solution with duct closed,  $\vec{V}_I$ .



(b) Axial-flow solution with duct open,  $\vec{V}_{II}$ .



(c) Crossflow flow solution with duct open,  $\vec{V}_{III}$ .

Figure 20. - Basic solutions for inlet.